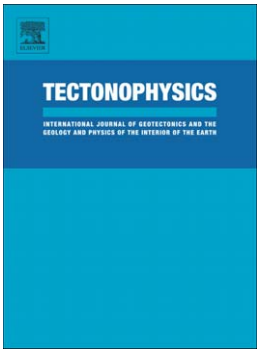

Crustal stress field perturbations in the continental margin around the Korean Peninsula and Japanese islands

Junhyung Lee, Tae-Kyung Hong, Chandong Chang

PII: S0040-1951(17)30320-7
DOI: doi: 10.1016/j.tecto.2017.08.003
Reference: TECTO 27577

To appear in: *Tectonophysics*

Received date: 10 November 2016
Revised date: 16 July 2017
Accepted date: 1 August 2017

Please cite this article as: Lee, Junhyung, Hong, Tae-Kyung, Chang, Chandong, Crustal stress field perturbations in the continental margin around the Korean Peninsula and Japanese islands, *Tectonophysics* (2017), doi: 10.1016/j.tecto.2017.08.003

Crustal stress field perturbations in the continental margin around the Korean Peninsula and Japanese islands

Junhyung Lee[a], Tae-Kyung Hong[a,*], and Chandong Chang[b]

Affiliation and address:

[a]Yonsei University, Department of Earth System Sciences, 50 Yonsei-ro, Seodaemun-gu Seoul 120-749, South Korea. (aqualung@yonsei.ac.kr, tkhong@yonsei.ac.kr)

[b] Chungnam National University, Department of Geology and Earth Environmental Sciences, Daejeon 305-764, South Korea. (cchang@cnu.ac.kr)

Corresponding author:

Tae-Kyung Hong

Abstract

Seismic activity and focal mechanisms are governed by the effective stress field that is a combined result of regional tectonic processes and local stress perturbation. This study investigates the regional variation in the stress field in the eastern continental margin of the Eurasian plate around the Korean Peninsula and Japanese islands using a damped stress inversion technique based on the focal mechanism solutions of regional earthquakes. The dominant compressional stress is directed ENE-WSW around the Korean Peninsula and eastern China, E-W at the central East Sea and northern and southern Japan, NW-SE at central Japan, and N-S around the northern Nankai trough. The dominant compression direction changes rapidly in the East Sea and Japanese islands, which may be due to the combined effects of tectonic loading in the subduction zones off the Japanese islands and the India-Eurasia plate boundary. The crustal stress fields around the subduction zones off the Japanese islands present characteristic depth-dependent orientations. The orientations of the largest horizontal stress components, σ_H, in the subduction zones are subparallel with the plate convergence directions at shallow depths. The σ_H orientations are observed to rotate clockwise with the depth owing to slab subduction and lithospheric deformation. The regional stress field around the Japanese islands was perturbed temporally by the 2011 M9.0 Tohoku-Oki megathrust earthquake. The regional stress field was recovered in a couple of years. The stress field and tectonic structures are mutually affected, causing stress field distortion and a localized mixture of earthquakes in different faulting types.

Key words: reference ambient stress model, Korea, Japan, continental margin

1 Introduction

Seismic activity is a result of medium response to ambient stress field that is primarily influenced by regional tectonics. The seismic hazard potentials of region are highly dependent on the regional stress field. Long-term stress loading produces earthquakes even in paleotectonic structures (Choi et al., 2012; Hong and Choi, 2012). It was indicated that local stress field vary before large earthquakes and volcanic eruptions (e.g., Roman et al., 2004; Bohnhoff et al., 2006). Also, large earthquakes and volcanic eruptions may perturb the regional stress field, which may cause changes in seismicity properties. It is crucial to understand the evolution of stress field to assess the seismic hazard potentials.

The composition of the stress components controls the faulting style. The vertical stress component in a stable intraplate region is mainly controlled by the gravity of the overburden medium. The horizontal stress component is influenced by tectonic loading. Crustal structures and existing faults may distort the ambient stress field locally (Bosworth and Strecker, 1997; Sassi and Faure, 1997; Homberg et al., 1997; Andeweg et al., 1999; Arlegui and Simón, 2001; Rivera and Kanamori, 2002; Yale, 2003; Vavryčuk, 2011). The local stress field may vary by location.

We can infer the ambient stress field from geological data (e.g., fault slip), focal mechanism solutions, and in-situ field measurements (Zoback and Zoback, 1980; Stock et al., 1985; Mount and Suppe, 1987; Obara et al., 2000; Zoback et al., 2003; Lin et al., 2010; Lin et al., 2011). However, it is difficult to estimate the representative regional stress field from a single observation. We may determine the representative regional stress fields from focal mechanism solutions (Assumpcao, 1992; Abers and Gephart, 2001; Balfour et al., 2005; Choi et al., 2012; Heidbach et al., 2010; Macchiavelli et al., 2012).

Michael (1984, 1987) solves a linearized problem with the assumption that shear tractions are comparable on rupture planes (SLFAST). The Focal Mechanism Stress Inversion method (FMSI) searches for the best-fitting stress parameters (Gephart and Forsyth 1984; Gephart 1990). Similarly, a damped stress inversion technique searches for a stress tensor that minimizes the error over the observed fault plane solutions (Hardebeck and Michael, 2006). A formal stress inversion (FSI) method performs a composite analysis of independent focal mechanism solutions (Martínez-Garzón et al., 2014).

The eastern margin of the Eurasian plate around the Korean Peninsula and Japanese islands experience complex tectonic processes including plate convergence and lithospheric counter-response, comprising a laterally varying stress field. We investigate the representative regional stress field around the Korean Peninsula and Japanese islands, which may be crucial for the mitigation of seismic hazards.

2 Geology and tectonics

The eastern margin of the Eurasian plate around the Korean Peninsula and Japanese islands is encompassed by the Okhotsk plate, Pacific plate, and Philippine Sea plate (Fig. 1). The Pacific plate and Philippine Sea plate are convergent with the Okhotsk plate and Eurasian plate in the eastern offshore of the Japanese islands (Hashimoto et al., 2009; Huang et al., 2011). Japan trench and Nankai trough are placed on the convergent boundaries. The northern half of the Japanese islands belong to the Okhotsk plate, and the other half is placed in the Eurasian plate. The convergence rate of the Pacific plate in the Japan trench is ∼91 mm/yr, and that of the Philippine Sea plate is ∼50 mm/yr (Seno et al., 1993; Ide, 2013). The plate convergence environment constructs a compressional stress regime over the eastern Eurasian plate.

The stresses induced from the plate convergent boundaries are transmitted into the Japanese islands and Korean Peninsula, causing high seismicity in northern China and the Japanese islands (Liu et al., 2007). On the other hand, the seismicity is mild in southern China and the Korean Peninsula (Brantley and Chung, 1991; Liu, 2001; Hong and Choi, 2012). Shallow seismicity is rarely observed in the East Sea (Sea of Japan) and northeastern Korean Peninsula.

The Pacific plate reaches at a depth of 660 km near the east coast of the Korean Peninsula and moves laterally over the 660-km discontinuity (Lee et al., 2014; Revenaugh and Sipkin, 1994; Tonegawa et al., 2005; Zhao et al., 2009). The frontal margin of tje Philippine Sea plate is located at a depth of 200 km beneath the southern Japanese islands. The dipping angles of the subducting Philippine Sea plate are gentle and as low as $<10^\circ$ to 20° beneath the Shikoku and Chugoku islands and increase to $>50^\circ$ beneath Kyushu (Furumura et al., 2014). Active

volcanoes construct a volcanic arc on the Japanese islands that is subparallel with the trench axes (Furumura et al., 2014).

3 Methods

We identify the fault type from the geometry of the compressional (P), tensional (T), and null (B) axes of the stress field (Frohlich, 1992; Hong and Choi, 2012). We define that strike-slip events have dip angles with respect to the B axes greater than 60°, normal-faulting events have dip angles with respect to the P axes greater than 60°, and reverse events have dip angles with respect to the T axes greater than 50°. The other events are classified to be odd-faulting events that may result from a combination of two or three focal mechanisms.

The P, T, and B axes are defined to be (Aki and Richards, 1980; Gasperini and Vannucci, 2003)

$$\begin{aligned} \mathbf{p}_i &= \frac{\mathbf{n}_i - \mathbf{d}_i}{\sqrt{2}}, \\ \mathbf{t}_i &= \frac{\mathbf{n}_i + \mathbf{d}_i}{\sqrt{2}}, \\ \mathbf{b}_i &= \mathbf{e}_{ijk}\mathbf{n}_j\mathbf{d}_k, \end{aligned} \tag{1}$$

where $\mathbf{p}$ is the unit P-axis vector, $\mathbf{t}$ is the unit T-axis vector, $\mathbf{b}$ is the unit B-axis vector, $\mathbf{n}$ is the unit vector normal to the fault plane, $\mathbf{d}$ is the unit slip vector, and $\mathbf{e}$ is the unit azimuth vector.

We calculate a regional stress field from the fault mechanism solutions of regional earthquakes using the spatial and temporal stress inversion (SATSI) algorithm with a damped inversion method that simultaneously inverts the stress in all subregions while minimizing of the difference in the stresses between adjacent subregions (Hardebeck and Michael, 2006; Martínez-Garzón et al., 2014). The method implements a bootstrapping technique to determine the representative stress components for a set of focal mechanism solutions. The bootstrap analysis produce randomly resampled data sets with an allowance for duplicate selections, which enables us to examine the stability of the inversion results (e.g., Efron and Tibshirani, 1986; Hong and Menke, 2008). The SATSI algorithm is useful for the construction of a representative continuous stress field over a wide region.

The observed focal mechanism solutions $\mathbf{d}$ satisfy

$$\mathbf{d} = \mathbf{G}\mathbf{m}, \tag{2}$$

where $\mathbf{G}$ is the data kernel matrix, and $\mathbf{m}$ is the representative stress tensor. The vector $\mathbf{d}$ can be written in terms of unit slip vectors:

$$\mathbf{d} = \begin{pmatrix} u_{11} \\ u_{12} \\ u_{13} \\ \cdots \\ u_{K1} \\ u_{K2} \\ u_{K3} \end{pmatrix}, \tag{3}$$

where u_{ki} (i=1,2,3) is the i-directional component of the unit slip vector for event k, and K is the number of events. The matrix $\mathbf{G}$ is given by

$$\mathbf{G} = \begin{pmatrix} n_{11} - n_{11}^3 + n_{11}n_{13}^2 & n_{12} - 2n_{11}^2 n_{12} & n_{13} - 2n_{11}^2 n_{13} & n_{11}n_{13}^2 - n_{11}n_{12}^2 & -2n_{11}n_{12}n_{13} \\ n_{12}n_{13}^2 - n_{12}n_{11}^2 & n_{11} - 2n_{12}^2 n_{11} & -2n_{11}n_{12}n_{13} & n_{12} - n_{12}^3 + n_{12}n_{13}^2 & n_{13} - 2n_{12}^2 n_{13} \\ n_{13}^3 - n_{13}n_{11}^2 - n_{13} & -2n_{11}n_{12}n_{13} & n_{11} - 2n_{13}^2 n_{11} & n_{13}^3 - n_{13}n_{12}^2 - n_{13} & n_{12} - 2n_{13}^2 n_{12} \\ \cdots & \cdots & \cdots & \cdots & \cdots \\ n_{K1} - n_{K1}^3 + n_{K1}n_{K3}^2 & n_{K2} - 2n_{K1}^2 n_{K2} & n_{K3} - 2n_{K1}^2 n_{K3} & n_{K1}n_{K3}^2 - n_{K1}n_{K2}^2 & -2n_{K1}n_{K2}n_{K3} \\ n_{K2}n_{K3}^2 - n_{K2}n_{K1}^2 & n_{K1} - 2n_{K2}^2 n_{K1} & -2n_{K1}n_{K2}n_{K3} & n_{K2} - n_{K2}^3 + n_{K2}n_{K3}^2 & n_{K3} - 2n_{K2}^2 n_{K3} \\ n_{K3}^3 - n_{K3}n_{K1}^2 - n_{K3} & -2n_{K1}n_{K2}n_{K3} & n_{K1} - 2n_{K3}^2 n_{K1} & n_{K3}^3 - n_{K3}n_{K2}^2 - n_{K3} & n_{K2} - 2n_{K3}^2 n_{K2} \end{pmatrix}, \tag{4}$$

and the vector $\mathbf{m}$ is

$$\mathbf{m} = \begin{pmatrix} \tau_{11} \\ \tau_{12} \\ \tau_{13} \\ \tau_{22} \\ \tau_{23} \end{pmatrix}, \tag{5}$$

where n_{kj} is the j-directional component of the unit fault normal vector of event k, and τ_{lm}

(l, m =1,2,3) is the stress tensor component. Here $\tau_{33} = -(\tau_{11} + \tau_{22})$ is assumed (Hardebeck and Michael, 2006).

We apply a Gaussian elimination approach to calculate a set of least-squares solutions that are tested using a bootstrap analysis. We determine a representative moment tensor solution that minimizes the error among the set of solutions. The principal stress components are composed of two horizontal components ($\sigma_H > \sigma_h$) and a vertical component (σ_V). The stress composition of a strike-slip event satisfies the condition $\sigma_H > \sigma_V > \sigma_h$, that of a reverse event satisfies the condition $\sigma_H > \sigma_h > \sigma_V$, and that of a normal-faulting event satisfies the condition $\sigma_V > \sigma_H > \sigma_h$. We deduce the maximum horizontal stress field from the horizontal stress components of events.

The stress ratio R presents the composition of stress components (e.g., Bohnhoff et al., 2006; Hong and Choi, 2012):

$$R = \frac{\sigma_1 - \sigma_2}{\sigma_1 - \sigma_3}, \tag{6}$$

where σ_j (j=1,2,3) is the magnitude of a principal stress component ($\sigma_1 > \sigma_2 > \sigma_3$). Here, the situation in which $R > 0.5$ suggests a transpressional regime, and that with $R < 0.5$ indicates a transtensional regime (Bohnhoff et al., 2006).

4 Data

We collect the focal mechanism solutions of earthquakes from available resources including the Global CMT catalog, F-net catalog, and earlier studies. The Global CMT catalog contains the information of events with magnitudes greater than or equal to 4.7 during 1976-2016. The F-net catalog includes events with magnitudes greater than or equal to 3.1 during 1997-2016. The focal mechanism solutions of local seismic events with magnitudes greater than M_L 1.8 around the Korean Peninsula are available in earlier studies (Choi et al., 2012; Hong et al., 2015). We constrain the focal depths of events to be less than 40 km to deduce the crustal stress field. The number of focal mechanism solutions collected in this study is 12,028.

The spatial coverage of the available data is dense over the region around Japanese islands, and low over the Korean Peninsula (Fig. 1). Moreover, only a few shallow-focus earthquakes

are available in the East Sea (Sea of Japan). We additionally analyze three events around the Korean Peninsula using a long-period waveform inversion (Fig. 2; Table 1). We implement a 1-D velocity model (Kennett et al., 2006).

The strike-slip events are dominant in the regions around the Korean Peninsula, the southern Japanese islands, and off the east coast of the central and northern Japanese islands (Fig. 3). Reverse earthquakes occur over the central and northern Japanese islands and around the subduction zones of the Pacific plate. Normal-faulting earthquakes are observed around the subduction zones of the Pacific plate.

5 Analysis

The number of available data points is low around the Korean Peninsula owing to low seismicity (Fig. 1). We discretize the study region by 2°-by-2° cells that overlap with adjacent cells by 1.0° in longitude and latitude. The regional stress field in each cell is assumed to be homogeneous. We invert the regional stress field ($\sigma_1 > \sigma_2 > \sigma_3$) from the focal mechanism solutions of events with focal depths less than 40 km using SATSI (Fig. 4).

We identify the horizontal and vertical stress components from the magnitudes and plunges of the inverted stress components. A pure vertical stress component (σ_V) has a plunge around 90°, and pure horizontal stress components ($\sigma_H > \sigma_h$) have plunges of ∼0°. The plunges of σ_1 are generally populated at low angles ($< 20°$), suggesting σ_H (Fig. 5). The dominant plunges of σ_2 and σ_3 are at low and high angles ($< 20°$, $> 70°$). The feature suggests that σ_2 and σ_3 are either σ_h or σ_V.

We find that stress field inversions based on small numbers (<8) of data points may produce unstable results (Hardebeck and Michael, 2006). We verify the stability of the inverted stress components using a bootstrap analysis (Efron and Tibshirani, 1986). We generated 2000 bootstrap resampled data sets. The best-fit solutions are determined in 95% confidence level. Fig. 6 presents the errors of stress-component orientations from bootstrap analysis. The standard errors of σ_1 are small in most regions, ranging between 0.37° and 1.99° around the Korean Peninsula and Japanese islands. The average is 0.95° and the standard deviation is 0.38°. The observation suggests that the σ_1 orientations are determined stably from the inversion.

The standard errors of σ_2 are small around the central Japan, and those of σ_3 are small around the Korean Peninsula. The standard errors of σ_2 range between 0.69° and 6.89° around the central Japan. The average is 2.54° and the standard deviation is 1.96°. The standard errors of σ_3 range between 0.53° and 1.95° around the Korean Peninsula. The average is 0.84° and the standard deviation is 0.25°. The small standard errors suggest stable determination of the stress components. We, however, find that the inverted σ_2 presents large standard errors around the Korean Peninsula and southern and northern Japanese islands. Also, the inverted σ_3 displays large standard errors in the northern Japanese islands.

We examine the spatial resolution and accuracy of inverted stress fields by comparing the results between different grid systems. We invert the stress fields based on 1°-by-1° cells for the region around the Japanese islands where a large number of event data sets are available (Fig. 7). We observe that the results based on 2°-by-2° cells with a 1° overlap with adjacent cells are consistent with those based on 1°-by-1° cells. This observation suggests that an inversion based on 2°-by-2° cells may allow a reasonable presentation of the regional stress field even in the plate margin around the Japanese islands.

6 Regional stress field

We observe that the stress ratios R are generally greater than 0.5 (i.e., transpressional) in the regions dominated by reverse events and lower than 0.5 (i.e., transtensional) in the regions of normal-faulting events (Fig. 8). The R values are 0.3-0.7 for the regions where strike-slip events are dominant. The plunges of σ_1 are generally less than $\sim$20° in most regions, suggesting the maximum horizontal stress component, σ_H. This observation suggests that the regional stress field is predominantly induced by the tectonic loading associated with the plate tectonics. The orientations of the maximum horizontal stress components change gradually with the distances from the plate boundaries (Fig. 9(a)). The horizontal compressional stress field is calculated by interpolating the observed σ_1 directions (Fig. 9(b)).

The σ_H is oriented EW to ENE around the Korean Peninsula and normal to the trench axis around the subduction zones off the Japanese islands. It is noteworthy that the σ_H orientations around the subduction zones re generally subparallel with the plate convergence directions. The observation suggests that the stress field is controlled by the relative plate

motions. The orientations of σ_H gradually change with the distance from the trench-axis toward the intraplate regime. The orientations of σ_H change rapidly in the East Sea, presenting high lateral variations in the stress field. The rare seismicity in the crust of East Sea may be ascribed to the high variation of σ_H orientations. The rapid lateral variation of stress field around the Korean Peninsula and Japanese islands may be associated with the relative influence of convergent plate motions. The eastern margin of the Eurasian plate around the Korean Peninsula and Japanese islands is encompassed by the Okhotsk plate, Pacific plate, and Philippine Sea plate. The plate convergence environment constitutes a compressive stress regime around the eastern Eurasian plate. The influence of each convergent plate may be dependent on the distance and convergent speed. The σ_H orientations around the Japanese islands agree with other studies (e.g., Zoback, 1992; Townend and Zoback, 2006; Heidbach et al., 2010; Yokota et al., 2015).

The influence of a megathrust earthquake on the regional stress field is investigated. We compare the inverted stress field before and after the 11 March 2011 M9.0 Tohoku-Oki earthquake. The stress field before the megathrust earthquake is inverted using the data sets for five years from 11 March 2006 to 10 March 2011. Moreover, the postseismic stress fields are calculated using the data sets for two years from 11 March 2011 to 10 March 2013 and those for three years from 11 March 2013 to 10 March 2016 (Fig. 10). The stress field was perturbed locally after the megathrust in some locations. We find that the perturbed regional stress field was recovered within two years after the megathrust. This observation suggests that the regional stress field perturbed by a megathrust is recovered with time. In addition, the stress field recovery allows us to estimate the regional stress field with data sets over entire time periods reasonably.

7 Vertical variation in the stress field around the Japanese islands

The crustal stress field induced by tectonic loading may be generally invariant with the depth in regions away from the plate boundaries. Crustal and tectonic structures may cause a local variation in the stress field (e.g., Homberg et al., 1997; Kattenhorn and Marshall, 2006). The stress perturbation induces earthquakes in different faulting types in small regions, which is

obvious in the subduction zones (Fig. 11). However, earthquakes in common faulting types appear to be clustered locally (Fig. 11). Such coexistence of earthquakes in different faulting types is found in other convergent plate boundaries including the northern Chilean fore arc and India-Eurasia plate boundary (e.g., Loveless et al., 2010; Karagianni et al., 2015).

The coexistence of earthquakes in different faulting types may be associated with a local stress perturbation by the locking of subducting slabs, slab-surface branching, elastic rebound, and laterally inhomogeneous buoyancy forces (Savage, 1983; Bohnhoff et al., 2006; Toda and Matsumura, 2006; Loveless et al., 2010; Kita et al., 2010; Lin et al., 2016). A vertical stress perturbation is also observed in volcanic regions (e.g., D'Auria and Massa, 2015).

The σ_1 orientations are invariant with the depth in the inland Japanese islands. On the other hand, the σ_1 orientations distinctively change vertically in the offshore regions around the subduction zones (Fig. 12(a)). The σ_1 orientations at depths less than 10 km are generally subparallel with the plate convergence directions. The σ_1 orientations appear to rotate clockwise with increasing depth. Similarly, the σ_2 orientations at shallow depths (<10 km) around the trenches are subparallel with the trench axes and the fast shear-wave polarization orientations (Okada et al., 1995; Nakajima and Hasegawa, 2004; Long and van der Hilst, 2005). However, the σ_2 orientations appear to rotate anticlockwise with increasing depth, unlike the σ_1 orientations (Fig. 12(b)).

The stress components around the subduction zones do not change only in horizontal orientations but also in vertical orientations (Fig. 13). The largest primary stress component σ_1 displays a vertical variation in the plunges around the subduction zones. The vertical variation in the σ_1 plunges appears to change with the distance from the trenches. However, the plunges of σ_1 are invariant with the depth in the inland Japanese islands.

It is noteworthy that the vertical variation in the stress field in subduction zones is generally consistent with in-situ measurements (Tobin et al., 2009; Chang et al., 2010; Song et al., 2011; Wu et al., 2012; Lewis et al., 2013; Lin et al., 2016). The vertical variation in the stress field suggests an effective local stress perturbation by slab subduction and lithospheric deformation. In particular, the stress field is highly affected by the geometry of crustal or tectonic structures in a low-friction environment with a high fluid pressure (Balfour et al., 2005), which may be effective in subduction zones.

8 Discussion and conclusions

We investigated the regional stress field in the continental margin around the Korean Peninsula and Japanese islands from the focal mechanism solutions of regional earthquakes. We identified the stress regime from the composition of the stress components. Different fault types of earthquakes occur in the same regions particularly around subduction zones, which may be difficult to expect under a constant stress field. The contemporary existence of different combinations of stress components may be associated with local medium deformation and stress perturbation by existing crustal structures.

The plunge distribution of the inverted stress components suggested that the largest primary stress component (σ_1) corresponded to the largest horizontal stress component (σ_H). The other stress components (σ_2, σ_3) corresponded to the lowest horizontal stress component (σ_h) or vertical stress component (σ_V) depending on the location. The σ_H orientations were consistent with the plate convergence directions around the subduction zones off the Japanese islands. The orientations of σ_H in the Japanese islands gradually changed with the distance from the trenches. The orientations of σ_H changed rapidly in the East Sea and were directed EW to ENE around the Korean Peninsula. The horizontal compression stress fields around the Korean Peninsula and inland Japanese islands may be a consequence of the combined effects of tectonic loading in the subduction zones off the Japanese islands (Japan trench, Nankai trough) and the India-Eurasia plate boundary.

The σ_1 orientations were invariant with the depth in the crusts around the Korean Peninsula and inland Japanese islands. The σ_1 orientations displayed a characteristic clockwise rotation with depth around the subduction zones. On the other hand, the σ_2 orientations presented an anticlockwise rotation with the depth. The rotations of the horizontal stress components may be a consequence of a local stress perturbation by slab subduction and lithospheric deformation.

The depth-dependent stress field and the complex mixture of earthquakes in different faulting types suggest that local crustal structures and tectonic processes play important roles in the construction of a stress field in the subduction zones. Moreover, the stress field and tectonic structures mutually affect each other, causing a stress field distortion that induces earthquakes in different faulting types in small regions. A megathrust earthquake may

perturb the regional stress field temporally, incorporating temporal changes in the seismicity properties. Comprehension of the local stress may be useful for understanding the potential seismic hazards in continental margins. Moreover, a megathrust earthquake may cause a temporal perturbation in a regional stress field, subsequently incorporating a change in the seismicity property (e.g., Hong et al., 2015).

Acknowledgements

We are grateful to Dr. Iswarya Samikannu and two anonymous reviewers for valuable review comments. This work was supported by the Korea Meteorological Administration Research and Development Program under Grant KMIPA 2015-7040 and by the Basic Science Research Program through the National Research Foundation of Korea (NRF) funded by the Ministry of Education (NRF-2015R1D1A1A01060198). Support from the Basic Research and Development Project of the Korea Institute of Geoscience and Mineral Resources (KIGAM, Project code No. GP2016-014) funded by the Ministry of Science, ICT and Future Planning, Korea is also acknowledged.

References

Abers, G. A., and J. W. Gephart (2001), Direct inversion of earthquake first motions for both the stress tensor and focal mechanisms and application to southern California, Journal of Geophysical Research, 106(B11), 26,523-26,540.

Aki, K., and P. G. Richards (1980), Quantitative Seismology, vol. 1. W. H. Freeman and Company, San Francisco, California.

Andeweg, B., G. D. Vicente, S. Clowtingh, J. Giner, and A. M. Martin (1999), Local stress fields and intraplate deformation of Iberia: variations in spatial and temporal interplay of regional stress sources, Tectonophysics, 305, 153-164.

Arlegui, L., and J. L. Simón (2001), Geometry and distribution of regional joint sets in a non-homogeneous stress field: case study in the Ebro basin (Spain), Journal of structural Geology, 23, 297-313.

Assumpcao, M. (1992), The Regional Intraplate Stress Field in South America, Journal of Geophysical Research, 97(B8), 11,889-11,903.

Balfour, N. J., M. K. Savage, and J. Townend (2005), Stress and crustal anisotropy in Marlborough, New Zealand: evidence for low fault strength and structure-controlled anisotropy, Geophysical Journal International, 163, 1-14.

Bohnhoff, M., H. Grosser, and G. Dresen (2006), Strain partitioning and stress rotation at the North Anatolian fault zone from aftershock focal mechanisms of the 1999 Izmit Mw = 7.4 earthquake, Geophysical Journal International, 166, 373-385.

Bosworth, W., and M. R. Strecker (1997), Stress field changes in the Afro-Arabian rift system during the Miocene to Recent period, Tectonophysics, 278, 47-62.

Brantley, B. J., and W.-Y. Chung (1991), Body-wave waveform constraints on the source parameters of the Yangjiang, China, earthquake of July 25, 1969: a devastating earthquake in a stable continental region, Pure and Applied Geophysics, 135(4), 529-543.

Chang, C., L. C. McNeill, J. C. Moore, W. Lin, M. Conin, and Y. Yamada (2010), In situ stress state in the Nankai accretionary wedge estimated from borehole wall failures, Geochemistry, Geophysics, Geosystems, 11(12), Q0AD04. http://dx.doi.org/10.1029/2010GC003261.

Choi, H., T.-K. Hong, X. He, and C.-E. Baag (2012), Seismic evidence for reverse activation of a paleo-rifting system in the East Sea (Sea of Japan), Tectonophysics, 572-573, 123-133.

D'Auria, L., and B. Massa (2015), Stress Inversion of Focal Mechanism Data Using a Bayesian Approach: A Novel Formulation of the Right Trihedra Methodm Seismological Research Letters, 86(3), 968-977.

Efron, B., and R. Tibshirani (1986), Bootstrap methods for standard errors, confidence intervals, and other measures of statistical accuracy, Statistical Science, 1, 54-75.

Frohlich, C. (1992), Triangle diagrams: ternary graphs to display similarity and diversity of earthquake focal mechanisms, Physics of the Earth and Planetary Interiors, 75, 193-198.

Furumura, T., T.-K. Hong, and B. L. N. Kennett (2014), Lg wave propagation in the area around Japan: observations and simulations, Progress in Earth and Planetary Science, 1:10, doi:10.1186/2197-4284-1-10.

Gasperini, P., and G. Vannucci (2003), FPSPACK: a package of FORTRAN subroutines to manage earthquake focal mechanism data, Computational Geosciences, 29, 893-901.

Gephart, J. (1990), Stress and the direction of slip on fault planes, Tectonics, 9, 845-858.

Gephart, J., and D. Forsyth (1984), An improved method for determining the regional stress tensor

using earthquake focal mechanism data: application to the San Fernando earthquake sequence, Journal of Geophysical Research, 89, 9305-9320.

Hardebeck, J. L., and A. J. Michael (2006), Damped regional-scale stress inversions: Methodology and examples for southern California and the Coalinga aftershock sequence, Journal of Geophysical Research, 111, B11310, doi 10.1029/2005JB004144.

Hashimoto, C., A. Noda, T. Sagiya, and M. Matsu'ura (2009), Interplate seismogenic zones along the Kuril-Japan trench inferred from GPS data inversion, Nature Geoscience, 2, 141-144.

Heidbach, O., M. Tingay, A. Barth, J. Reinecker, D. Kurfeß, and B. Müller (2010), Global crustal stress pattern based on the World Stress Map database release 2008, Tectonophysics, 482, 3-15.

Homberg, C., J. C. Hu, J. Angelier, F. Bergerat, and O. Lacombe (1997), Characterization of stress perturbations near major fault zones: insights from 2-D distinct-element numerical modelling and field studies (Jura mountains), Journal of Structural Geology, 19(5), 703-718.

Hong, T.-K., and H. Choi (2012), Seismological constraints on the collision belt between the North and South China blocks in the Yellow Sea, Tectonophysics, 570-571, 102-113.

Hong, T.-K., J. Lee, and S. E. Houng (2015), Long-term evolution of intraplate seismicity in stress shadows after a megathrust, Physics of the Earth and Planetary Interiors, 245, 59-70.

Hong, T.-K., and W. Menke (2008), Imaging laterally varying regional heterogeneities from seismic coda using a source-array analysis, Physics of the Earth and Planetary Interiors, 166, 188-202.

Huang, Z., L. Wang, D. Zhao, N. Mi, and M. Xum (2011), Seismic anisotropy and mantle dynamics beneath China, Progress in Earth and Planetary Science Letters, 306, 105-117.

Ide, S. (2013), The proportionality between relative plate velocity and seismicity in subduction zones, Nature Geoscience, 6, 780-784.

Karagianni, I., C. B. Papazachos, E. M. Scordilis, and G. F. Karakaisis (2015), Reviewing the active stress field in Central Asia by using a modified stress tensor approach, Journal of Seismology, 19(2), 541-565.

Kattenhorn, S. A., and S.T. Marshall (2006), Fault-induced perturbed stress fields and associated tensile and compressive deformation at fault tips in the ice shell of Europa: implications for fault mechanics, Journal of Structural Geology, 28, 2204-2221.

Kennett, B. L. N., E. R. Engdahl, and R. Buland (1995), Constraints on seismic velocities in the earth from travel times, Geophysical Journal International, 122 (1), 108-124.

Kita, S., T. Okada, A. Hasegawa, J. Nakajima, and T. Matsuzawa (2010), Existence of interplane earthquakes and neutral stress boundary between the upper and lower planes of the double seismic zone beneath Tohoku and Hokkaido, northeastern Japan, Tectonophysics, 496, 68-82.

Lee, S.-H., J. Rhie, Y. Park, and K.-H. Kim (2014), Topography of the 410 and 660 km discontinuities beneath the Korean Peninsula and southwestern Japan using teleseismic receiver functions, Journal of Geophysical Research, 119(9), 7245-7257.

Lewis, J., T. Byrne, abd K. Kanagawa (2013), Evidence for mechanical decoupling of the upper plate at the Nankai subduction zone: constraints from core-scale faults at NantroSEIZE Sites C0001 and C0002, Geochemistry, Geophysics, Geosystems, 14(3), 620-633.

Lin, W.R., M.-L. Doan, J. C. Moore, L. McNeill, T. B. Byrne, T. Ito, D. Saffer, M. Conin, and the IODP Expedition 319 Scientific Party (2010), Present-day principal horizontal stress orientations in the Kumano forearc basin of the southwest Japan subduction zone determined from IODP NanTroSEIZE drilling Site C0009, Geophysical Research Letters, 37, L13303, doi.org/10.1029/2010GL043158.

Lin, W., S. Saito, Y. Sanada, Y. Yamamoto, Y. Hashimoto, and T. Kanamatsu (2011), Principal horizontal stress orientations prior to the 2011 Mw 9.0 Tohoku-Oki, Japan, earthquake in its source area, Geophysical Research Letters, 38, L00G10, doi:10.1029/2011GL049097.

Lin, W., T. B., Byrne, M. Kinoshita, L. C. McNeill, C. Chang, J. C. Lewis, Y. Yamamoto, D. M. Saffer, J. C. Moore, H.-Y. Wu, T. Tsuji, Y. Yamada, M. Conin, S. Saito, T. Ito, H. J. Tobin, G. Kimura, K. Kanagawa, J. Ashi, M. B. Underwood, and T. Kanamatsu (2016), Distribution of stress state in the Nankai subduction zone, southwest Japan and a comparison with Japan Trench, Tectonophysics, 692, 120-130.

Liu, L. (2001), Stable continental region earthquakes in South China, Pure and Applied Geophysics, 158, 1583-1611.

Liu, M., Y. Yang, Z. Shen, S. Wang, M. Wang, and Y. Wan (2007), Active tectonics and intracontinental earthquakes in China: the kinematics and geodynamics, Geological Society of America Special Paper, 425, 209-318.

Long, M. D., and R. D. van der Hilst (2005), Upper mantle anisotropy beneath Japan from shear wave splitting, Physics of the Earth and Planetary Interiors, 151, 206-222.

Loveless, J. P., R. W. Allmendinger, M. E. Pritchard, and G. González (2010), Normal and reverse faulting driven by the subduction zone earthquake cycle in the northern Chilean fore arc, Tectonics, 29, TC2001, doi:10.1029/2009TC002465.

Macchiavelli, C., S. Mazzoli, A. Megna, F. Saggese, S. Santini, and S. Vitale (2012), Applying the Multiple Inverse Method to the analysis of earthquake focal mechanism data: New insights into the active stress field of Italy and surrounding regions, Tectonophysics, 580, 124-149.

Martínez-Garzón, P., G. Kwiatek, M. Ickrath, and M. Bohnhoff (2014), MSATSI: A MATLAB package

for stress inversion combining solid classic methodology, a new simplified user-handling, and a visualization tool, Seismological Research Letters, 85, 896-904.

Michael, A. (1984), Determination of stress from slip data: faults and folds, Journal of Geophysical Research, 89, 11,517-11,526.

Michael, A. (1987), Use of focal mechanisms to determine stress: a control study, Journal of Geophysical Research, 92, 357-368.

Mount V. S., and J. Suppe (1987), State of stress near the San Andreas fault: Implications for wrench tectonics, Geology, 15, 1143-1146.

Nakajima, J., and A. Hasegawa (2004), Shear-wave polarization anisotropy and subduction-induced flow in the mantle wedge of northeastern Japan, Earth and Planeatary Science Letters, 225, 365-377.

Obara, Y., N. Nakamura, S. S. Kang, and K. Kaneko (2000), Measurement of local stress and estimation of regional stress associated with stability assessment of an open-pit rock slope, International Journal of Rock Mechanics and Mining Sciences, 37, 1211-1221.

Okada, T., T. Matsuzawa, and A. Hasegawa (1995), Shear-wave polarization anisotropy beneath the north-eastern part of Honshu, Japan, Geophysical Journal International, 123, 781-797.

Revenaugh, J., and S. A. Sipkin (1994), Mantle discontinuity structure beneath China, Journal of Geophysical Research, 99(B11), 21,911-21,927.

Rivera, L., and H. Kanamori (2002), Spatial heterogeneity of tectonic stress and friction in the crust, Geophysical Research Letters, 29(6), 1088, doi:10.1029/2001GL013803.

Roman, D. C., S. C. Moran, J. A. Power, K. V. Cashman (2004), Temporal and spatial variation of local stress fields before and after the 1992 eruptions of Crater Peak vent, Mount Spurr volcano, Alaska, Bulletin of the Seismological Society of America, 94, 2366-2379.

Sassi, W., and J.-L. Faure (1996), Role of faults and layer interfaces on the spatial variation of stress regimes in basins: inferences from numerical modelling, Tectonophysics, 266, 101-119.

Savage, J. C. (1983), A dislocation model of strain accumulation and release at a subduction zone, Journal of Geophysical Research, 88(B6), 4984-4996.

Seno, T., S. Stein, and A. E. Gripp (1993), A model for the motion of the Philippine Sea plate consistent with NUVEL-1 and geological data, Journal of Geophysical Research, 98, 17,941-17,948.

Song, I., D. M. Saffer, P. B. Flemings (2011), Mechanical characterization of slope sediments: constraints on in situ stress and pore pressure near the tip of the megasplay fault in the Nankai accretionary complex, Geochemistry, Geophysics, Geosystems, 12, Q0AD17. http://dx.doi.org/10.1029/2011GC003556.

Stock, J. M., J. H. Healy, S. H. Hickman, and M. D. Zoback (1985), Hydraulic Fracturing Stress

Measurements at Yucca Mountain, Nevada, and Relation ship to the Regional stress Field, Journal of Geophysical Research, 90(B10), 8691-8706.

Tobin, H., M. Kinoshita, J. Ashi, S. Lallemant, G. Kimura, E. Screaton, M. Kywa Thu, H. Masago, D. Curewitz, and IODP Expeditions 314/315/316 Scientific Party (2009), NanTroSEIZE Stage 1 Expeditions 314, 315, and 316: First Drilling Program of the Nankai Trough Seismogenic Zone Experiment, Scientific Drilling, 8, 4-17, doi:10.2204/iodp.sd.8.01.2009, 2009.

Toda, S., and S. Matsumura (2006), Spatio-temporal stress states estimated from seismicity rate changes in the Tokai region, central Japan, Tectonophysics, 417, 53-68.

Tonegawa, T., K. Hirahara, and T. Shibutani (2005), Detailed structure of the upper mantle discontinuities around the Japan subduction zone imaged by receiver function analyses, Earth Planets Space, 57, 5-14.

Townend, J., and M. D. Zoback (2006), Stress, strain, and mountain building in central Japan, Journal of Geophysical Research, 111, B03411, doi:10.1029/2005JB003759.

Vavryčuk, V. (2011), Principal earthquakes: Theory and observations from the 2008 West Bohemia swarm, Earth and Planetary Science Letters, 305, 290-296.

Wu, H.-Y., M. Kinoshita, and Y. Sanada (2012), Stress state estimation by geophysical logs in NanTroSEIZE Expedition 319-Site C0009, Kumano Basin, southwest Japan, Geophtsical Research Letters, 39, L18303, doi:10.1029/2012GL053086.

Yale, D. P. (2003), Fault and stress magnitude controls on variations in the orientation in situ stress fracture and in-situ stress characterization of hydrocarbon reservoirs, Geological Society, London, Special Publications, 209, 55-64.

Yokota, Y., T. Ishikawa, M. Sato, S. Watanabe, H. Saito, N. Ujihara, Y. Matsumoto, S. Toyama, M. Fujita, T. Yabuki, M. Mochizuke, and A. Asada (2015), Heterogeneous interplate coupling along the Nankai Trough, Japan, detected by GPS-acoustic seafloor geodetic observation, Progress in Earth and Planetary Science, 2(1), 10.

Zhao, D., Y. Tian, J. Lei, L. Liu, and S. Zheng (2009), Seismic image and origin of the Changbai intraplate volcano in East Asia: Role of big mantle wedge above the stagnant Pacific slab, Physics of the Earth and Planetary Interiors, 173, 197-206.

Zoback, M. D., C. A. Barton, M. Brudy, D. A. Castillo, T. Finkbeiner, B.R. Grollimund, D.B. Moos, P. Peska, C.D. Ward, and D.J. Wiprut (2003), Determination of stress orientation and magnitude in deep wells, International Journal of Rock Mechanics and Mining Sciences, 40, 1049-1076.

Zoback, M. L. (1992), First-and second-order patterns of stress in the lithosphere: The World Stress Map Project, Journal of Geophysical Research, 97(B8), 11,703-11,728.

Zoback, M. L., and M. Zoback (1980), State of Stress in the Conterminous United States, Journal of Geophysical Research, 85(B11), 6113-6156.

Table 1. Source parameters and fault-plane solutions of regional earthquakes around the Korean Peninsula that were analyzed additionally using long-period waveform inversion.

date (yyyy-mm-dd)	time (hh:mm:ss)	lat (°N)	lon (°E)	dep (km)	M_L	M_w	strike (°)	dip (°)	rake (°)	N
2013-05-17*	18:00:58*	37.675§	124.610§	6†	3.5*	3.6†	105†	85†	-29†	6
2013-05-18*	02:45:15*	37.677§	124.630§	5†	3.9*	4.0†	280†	90†	20†	7
2013-09-11*	04:00:31*	33.56*	125.39*	8†	4.0*	3.7†	40†	88†	175†	7

∗: parameter collected from an earthquake catalog of a local institute (KMA)

§: parameter determined by a locationing method (HYPOINVERSE)

†: parameter determined by waveform inversion

M_L: local magnitude

M_w: moment magnitude

N: number of data points used for waveform inversion

Figures

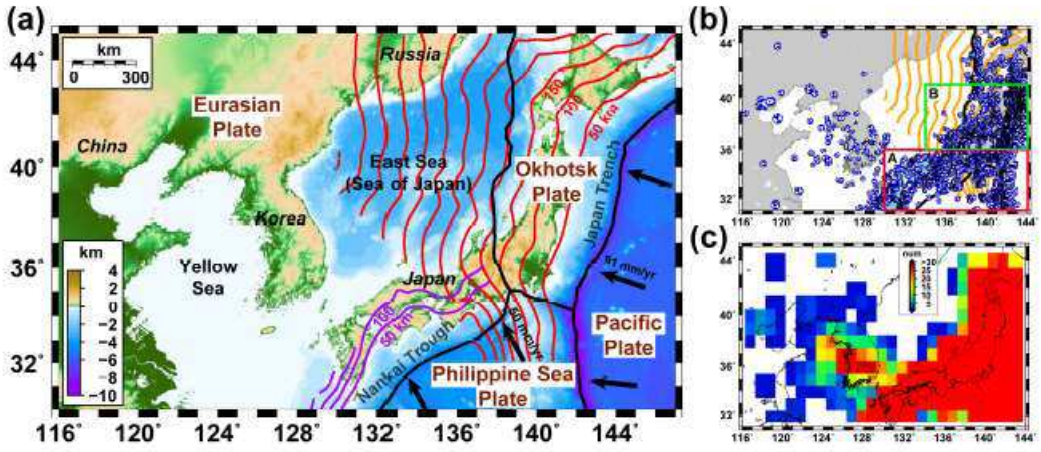

Figure 1. (a) Map of the region around the Korean Peninsula and Japanese islands. The major tectonic structures are presented. The depths of subducting slabs are marked with contours. The plate convergence directions and speeds are presented. (b) Spatial distribution of focal mechanism solutions of events. Two trench regions (A, B) are marked with solid lines. (c) Numbers of events over the discrete cells of a region. The numbers are high in the Japanese islands and Korean Peninsula.

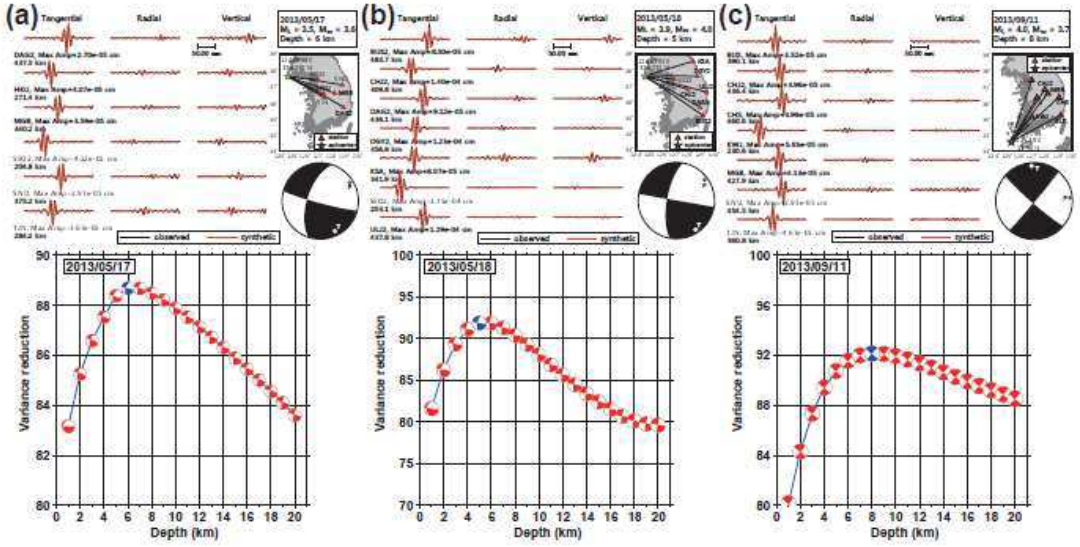

Figure 2. Long-period waveform inversion of three events around the Korean Peninsula: (a) the 17 May 2013 M_L3.5 earthquake, (b) the 18 May 18 2013 M_L3.9 earthquake, and (c) the 11 September 2013 M_L4.0 earthquake. The observed seismic waveforms are compared with synthetic waveforms. A map of stations and the inverted focal mechanism solutions are presented. The variance reduction as a function of the depth is displayed.

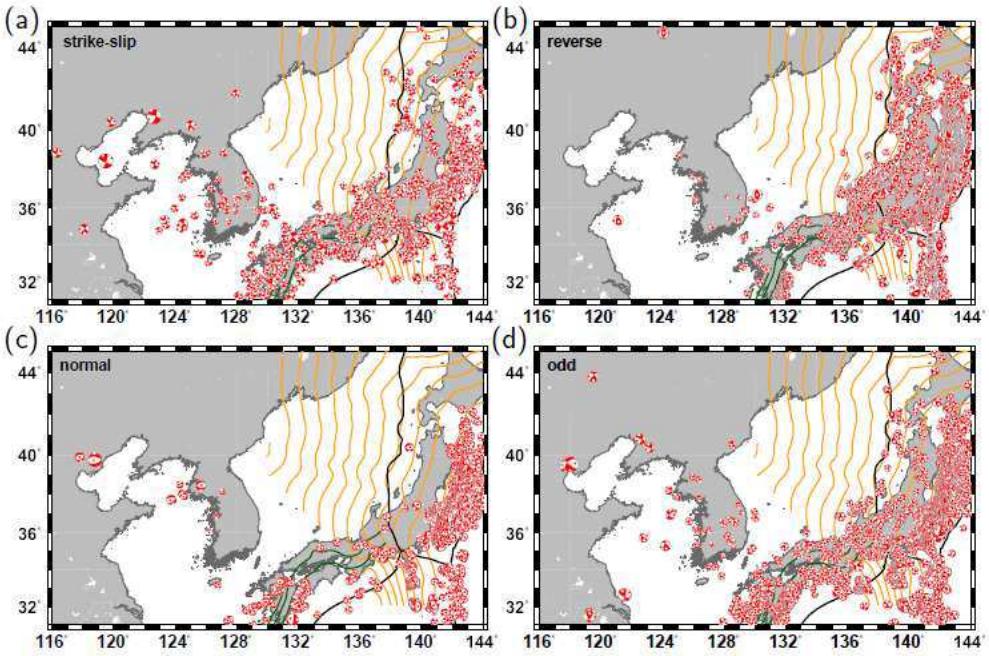

Figure 3. Spatial distribution of earthquakes: (a) strike-slip events, (b) reverse events, (c) normal-faulting events, and (d) odd-faulting events. Strike-slip events are dominant in the region around the Korean Peninsula. Normal-faulting events are observed in the trench regions and east coast of the Japanese islands. Reverse events are dominant around the Japanese islands.

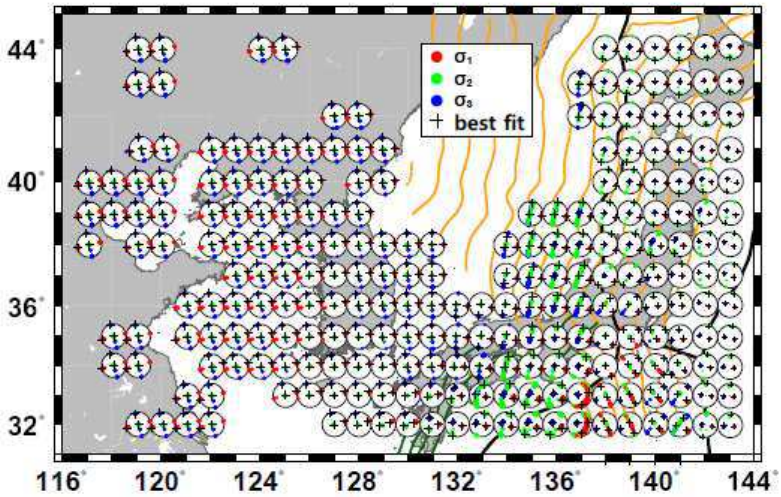

Figure 4. Stress components inverted from the focal mechanism solutions of regional earthquakes. The sets of inverted stress components from a bootstrap analysis are presented, and the best-fit result is marked with crosses.

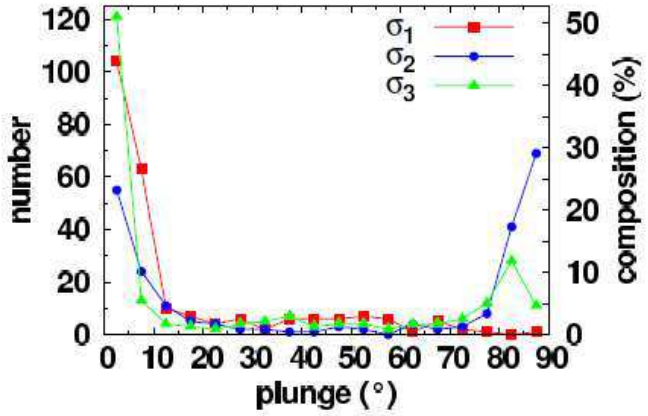

Figure 5. Distribution of plunges of inverted stress components $(\sigma_1, \sigma_2, \sigma_3)$. The plunges of σ_1 are populated at angles less than $\sim 20°$. The plunges of σ_2 and σ_3 are clustered at angles less than $\sim 20°$ and greater than $\sim 70°$.

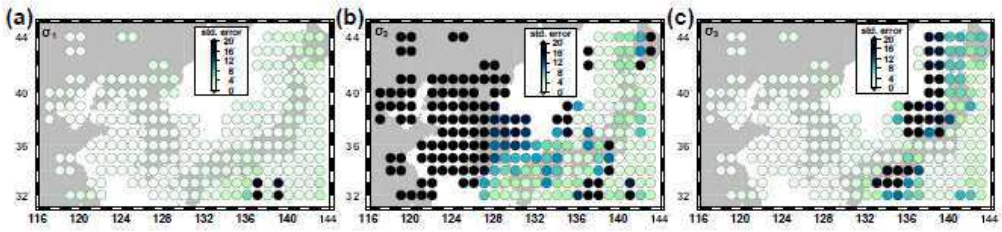

Figure 6. Standard errors of the stress-component orientations from a bootstrap analysis of the stress field inversions. The standard errors of σ_1 are small in most regions. The standard errors of σ_2 are small around the Japanese islands, and those of σ_3 are small in most regions except the northern Japanese islands.

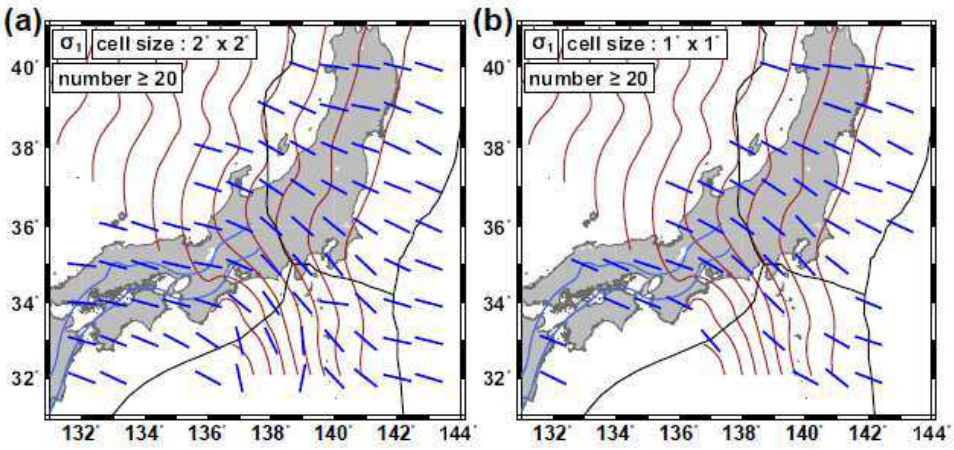

Figure 7. Inverted σ_1 orientations around the Japanese islands: results based on (a) 2°-by-2° spatial bins and (b) 1°-by-1° spatial bins. The inverted σ_1 orientations are similar for the two spatial-bin systems.

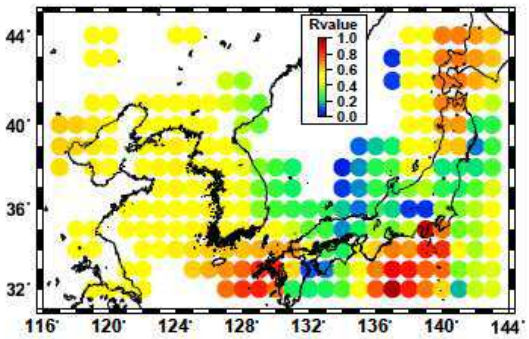

Figure 8. Distribution of the stress ratios (R). The stress ratios are 0.3-0.6 around the Korean Peninsula and vary widely around the Japanese islands.

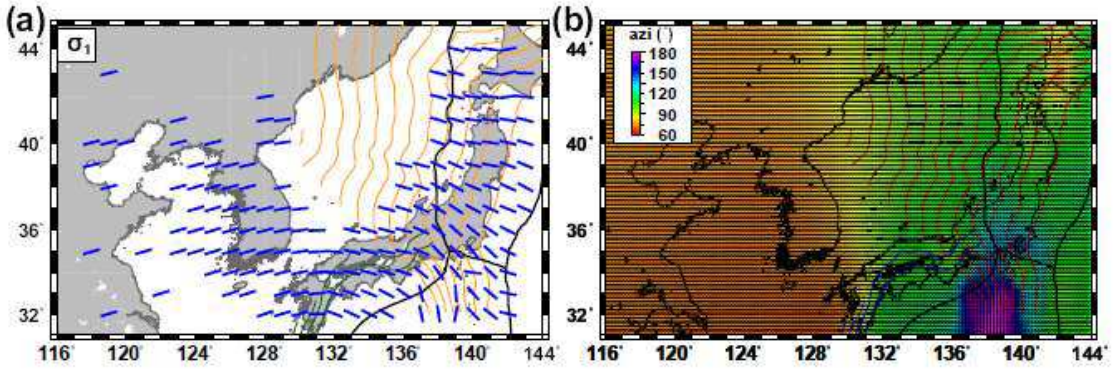

Figure 9. (a) Orientations of the largest horizontal stress components (σ_1) at discrete spatial bins and (b) the interpolated σ_1 field. The σ_1 field is oriented EW to ENE around the Korean Peninsula and trench-normal around the subduction zones off the Japanese islands.

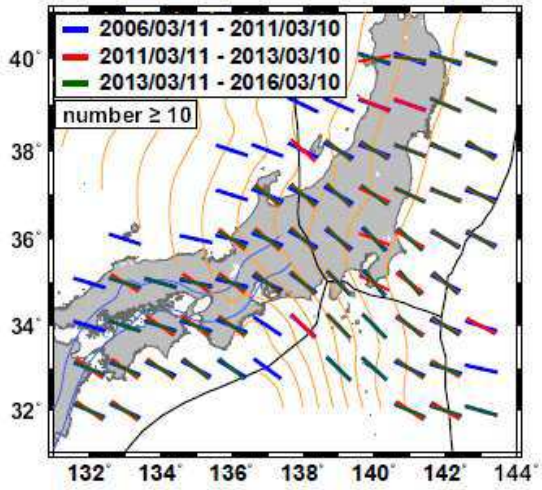

Figure 10. Comparison of the regional stress fields (σ_1) before and after the 11 March 2011 M9.0 Tohoku-Oki earthquake. The regional stress field was perturbed temporally after the megathrust. The stress field was recovered two years after the megathrust.

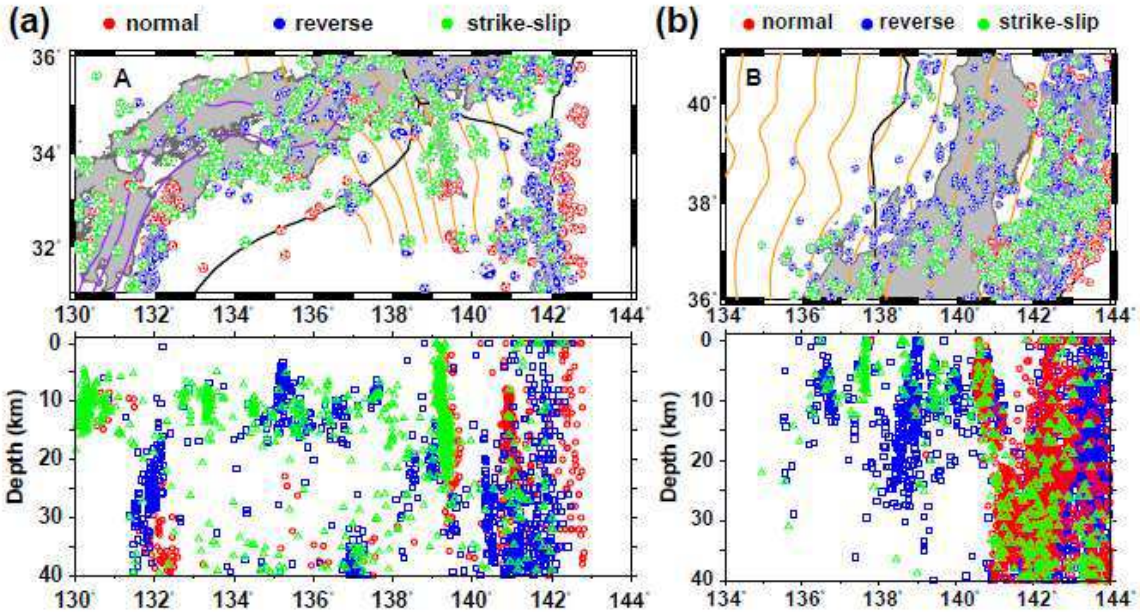

Figure 11. Lateral and vertical distributions of events for regions (a) A and (b) B.

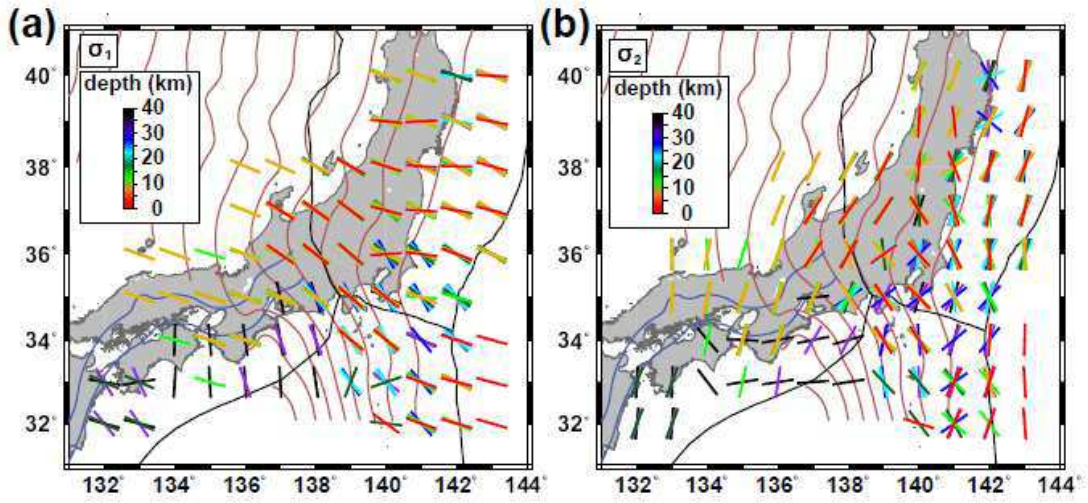

Figure 12. Vertical variations in the stress-component orientations (a) σ_1 and (b) σ_2. The orientations of the stress components are invariant with the depth in the inland regions. The stress-component orientations change with the depth around the subduction zones off the Japanese islands.

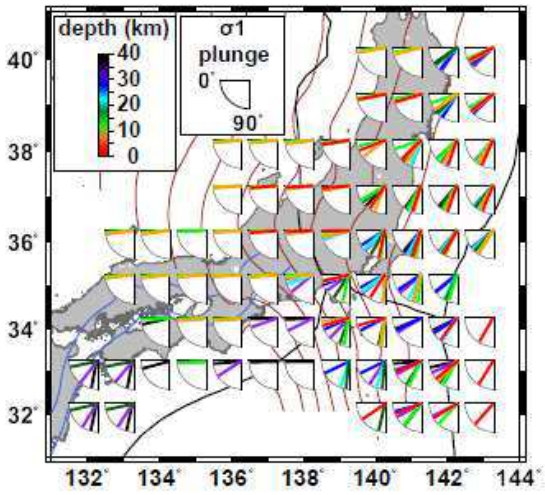

Figure 13. Vertical distribution of σ_1 plunges around the Japanese islands. The σ_1 plunges are invariant with the depth in the inland regions and change with the depth around the subduction zones.

Highlights

- The regional stress field around the eastern Eurasian plate margin displays large lateral and vertical variations.
- Crustal and tectonic structures deform the local stress fields.
- A megathrust earthquake perturbs the regional stress field that is recovered in a couple of years.